Multi-Scale Validation of MODIS LAI Products Based on Crop Growth Period

Ting Wang [1], Yonghua Qu [2,3,4], Ziqing Xia [1], Yiping Peng [1] and Zhenhua Liu [1,*]

[1] College of Natural Resources and Environment, South China Agricultural University, Guangzhou 510642, China; wt@stu.scau.edu.cn (T.W.); xzq@stu.scau.edu.cn (Z.X.); pyppyp@stu.scau.edu.cn (Y.P.)

[2] State Key Laboratory of Remote Sensing Science, Jointly Sponsored by Beijing Normal University and the Institute of Remote Sensing Applications of CAS, Beijing 100875, China; qyh@bnu.edu.cn

[3] Beijing Key Laboratory for Remote Sensing of Environment and Digital Cities, Beijing Normal University, Beijing 100875, China

[4] School of Geography, Beijing Normal University, Beijing 100875, China

* Correspondence: zhenhua@scau.edu.cn; Tel.: +86-135-3943-3693

check for updates

Abstract: Leaf area index (LAI) is one of the most important canopy structure parameters utilized in process-based models of climate, hydrology, and biogeochemistry. In order to determine the reliability and applicability of satellite LAI products, it is critical to validate satellite LAI products. Due to surface heterogeneity and scale effects, it is difficult to validate the accuracy of LAI products. In order to improve the spatio-temporal accuracy of satellite LAI products, we propose a new multi-scale LAI product validation method based on a crop growth cycle. In this method, we used the PROSAIL model to derive Advanced Spaceborne Thermal Emission and Reflection Radiometer (ASTER) LAI data and Gaofen-1 (GF-1) for the study area. The Empirical Bayes Kriging (EBK) interpolation method was used to perform a spatial multi-scale transformation of Moderate Resolution Imaging Spectroradiometer (MODIS) LAI products, GF-1 LAI data, and ASTER LAI data. Finally, MODIS LAI satellite products were compared with field measured LAI data, GF-1 LAI data, and ASTER LAI data during the growing season of crop field. This study was conducted in the agricultural oasis area of the middle reaches of the Heihe River Basin in northwestern China and the Conghua District of Guangzhou in Guangdong Province. The results suggest that the validation accuracy of the multi-scale MODIS LAI products validated by ASTER LAI data were higher than those of the GF-1 LAI data and the reference field measured LAI data, showing a R^2 of 0.758 and relative mean square error (RRMSE) of 28.73% for 15 m ASTER LAI and a R^2 of 0.703 and RRMSE of 30.80% for 500 m ASTER LAI, which imply that the 15 m MODIS LAI product generated by the EBK method was more accurate than the 500 m and 8 m products. This study provides a new validation method for satellite remotely sensed products.

Keywords: multi-scale LAI product validation; PROSAIL model; EBK; crop growth period

1. Introduction

Leaf area index (LAI) plays an important role in the biophysical processes of vegetation canopies and exchange processes of matter and energy between the Earth and atmosphere [1–4]. With advances in remote sensing technology, a number of satellite LAI products have been generated to monitor regional and global vegetation. Among them, the Moderate Resolution Imaging Spectroradiometer (MODIS) LAI product has been widely used. However, the availability of satellite products for scientific research and practical applications presents uncertainties due to various effects such as model algorithm, observation conditions, and sensor specifications [5]. Thus, it is important to validate the accuracy of LAI satellite products for assuring their effective utility in various disciplines [6].

Methods for the validation of LAI products are divided into three types: product intercomparison, direct validation, and indirect validation [7,8]. Product intercomparisons are conducted to evaluate the relative accuracy of satellite LAI products by comparing the spatio-temporal consistency among different satellite LAI products with similar time phase, same projection coordinate system, and spatial resolution [9]. Garrigues et al. [7] investigated the performances and spatio-temporal consistencies of four major global LAI products at 1/11.2° spatial sampling and a monthly time step: ECOCLIMAP climatology, GLOBCARBON (GLOBal Biophysical Products Terrestial CARBON Studies), CYCLOPES (Carbon Cycle and Change in Land Observational Products from an Ensemble of Satellites), and MODIS Collection 4. Yang et al. [9] compared and analyzed the spatio-temporal consistency of GEOV1 (GEOLAND2 Version 1), GLASS (Global Land Surface Satellite), and MODIS LAI products in southwest China's mountainous area. A product intercomparison can easily be achieved over a large number of sites representing the global distribution of land surface types and over a complete vegetation cycle. However, the product intercomparison method does not utilize concurrent field measurement data to evaluate the spatio-temporal consistencies of different products [7,8,10]. Thus, this approach cannot guarantee the absolute accuracy of satellite products [11].

The direct verification method considers ground measurements as the reference against which to evaluate the precision of satellite products. Sea et al. [12] compared MODIS LAI collections 4.8 and 5.0 with ground-based measurements taken along a 900 km north–south transect through the savanna in the Northern Territory of Australia. Fang et al. [8] verified MODIS LAI and CYCLOPES LAI using global field measured data and suggested that the direct comparison method is promising when a sufficient number of ground points are used and the field is homogeneous over a large area. However, it is difficult to satisfy this surface homogeneity requirement when validating estimates from remote sensing images with larger pixel size because vegetation cover is rarely uniform over large areas [13–15].

The indirect validation method is a more reasonable approach for validating low-resolution satellite products because it can avoid the spatial scale-mismatch problem [16]. The method builds a "bridge" between ground measured data and low-resolution remote sensing products using relatively high resolution satellite or aerial remote sensing images. Yang et al. [17] verified the accuracy of MODIS LAI products in the Qinghai Lake Basin by using Landsat 8 OLI data combined with field measurement data. They resampled the 30 m Landsat 8 LAI products into 1 km pixels to compare them to the MOD15A2 product, pixel by pixel. However, few studies [18,19] have been able to downscale the lower spatial resolution satellite LAI products into the spatial resolution of the bridging LAI results and then conduct a comparison, as it is difficult to generate LAI products with lower resolution without a sufficient number of homogeneous samples.

These existing validation efforts suggest that the present methods cannot determine the applicable scale of the LAI satellite product only based on the accuracy of the validation of the satellite product with the original resolution. As one of the most important canopy structure parameters in process-based models of crop biogeochemistry, LAI reflects crop growth characteristics. In order to quickly and efficiently monitor crop growth, it is very important to validate MODIS LAI products on crop growth period. The existing validation methods also rarely consider the crop growth cycle, which reduces the reliability of the verification accuracy. The objective of this study was to build a new validation method based on the Empirical Bayes Kriging (EBK) interpolation and the crop growth cycle to verify the accuracy of multi-scale MODIS LAI products. Taking an oasis agricultural area in the middle reaches of the Heihe River Basin and the Conghua District of Guangzhou in Guangdong Province as examples, the method used the PROSAIL model and Advanced Spaceborne Thermal Emission and Reflection Radiometer (ASTER) images and the Gaofen-1 (GF-1) images to produce ASTER LAI and GF-1 LAI reference maps. Then, the EBK interpolation method was driven to perform spatial upscaling transformations on ASTER LAI from 15 m spatial resolution to 500 m, GF-1 LAI from 8 m to 500 m and spatial downscaling transformation on the MODIS LAI images from 500 m spatial resolution to 15 m

and 8 m. Finally, the multitemporal and spatial scale LAI product validation was completed on the crop during its crop growth cycle.

## 2. Materials and Methods

2.1. Study Area

This study dealt with both the agricultural oasis area of the middle reaches of the Heihe River Basin (Figure 1b,c) and the Conghua District of Guangzhou in Guangdong Province (Figure 1d,e). The agricultural oasis area of the middle reaches of the Heihe River Basin is located in northwestern China with the latitude and longitude ranges of 38° to 42° N and 98° to 101°30′ E. It has a temperate continental climate, with short and hot summers, long and cold winters, an annual precipitation of only 54.9~436.2 mm, and annual evaporation of 1700 mm. Due to pressure on water resources in this fragile ecological environment, it is critical to monitor surface vegetation cover and vegetation growth of this agricultural oasis district in the Heihe River Basin. Satellite LAI products offer a means to efficiently monitor vegetation cover over larger regions, but to do this reliably, it is necessary to validate their accuracy. Additionally, Conghua District of Guangzhou City, China (11,317′–11,404′ E, 2322′–2356′ N) is located in the transition zone from the Pearl River Delta to the northern mountain area of Guangzhou. It has a humid subtropical monsoon climate characterized by warm winters, hot summers, little frost and snow, and sufficient rain and sunshine. The annual average temperature is 21.6 °C, and the annual precipitation is 2176.3 mm. Rice is one of the major crops in the study area and a year can be planted in two seasons.

2.2. Data and Pre-Processing

A total of 121 samples were collected from corn during the 2012 growing season on 24 May, 15 June, 23 June, 10 July, 3 August, 12 August, 18 August, 27 August, and 20 September. The measured samples including LAI, leaf angle distribution (LAD), chlorophyll a and b content (Cab) spectral data were provided by Heihe Plan Science Data Center, National Natural Science Foundation of China [20–22]. In the Conghua District of Guangzhou City, a total of 100 samples (green points in Figure 1e) were collected on 3 August, 17 September, 26 September, 15 October, and 24 October in 2015a. In order to meet the validation requirements for the MODIS LAI product at 500 m spatial resolution, field sampling plots of 0.5 km by 0.5 km were designed and within each plot, the LAI were collected by LAI-2000 Plant Canopy Analyzers (LI-COR, Inc., Lincoln, NE, USA) at five locations. Additionally, the values at the five locations were averaged for each sampling plot. One of the five points was located at the center of the plot, and the other four points were located at equal distances along the diagonal. Other parameters used in the PROSAIL model were derived from the Leaf Optical Properties Experiment 93 (LOPEX93) database including leaf structure parameter, pigment content, water content, and content of other components. Figure 1 shows the distribution of the sample points collected on 10 July 2012.

To validate the performance of our approach, we obtained images from the MOD15A2H LAI products, GF-1, and ASTER. Additionally, to avoid the combined effect of soil background value and vegetation, the MODIS LAI, GF-1, and ASTER images were selected for the same time phase with the measured LAI data We used the MODIS Reprojection Tool to transform the MODIS LAI data from Sinusoidal to UTM-WGS84 projection and applied the scaling factor of 0.1 [23] to obtain the standard MODIS LAI. The ASTER data and GF-1 data were geometrically corrected with a total of 24 ground control points measured using global positioning system (GPS) and applying a least squares transformation. The root mean square error (RMSE) between the estimated and measured ground control points was less than 0.5 pixel. Atmospheric corrections of ASTER data and GF-1 data were conducted using the FLAASH model. Geometric corrections for the MODIS products were performed with the MODIS Tools software.
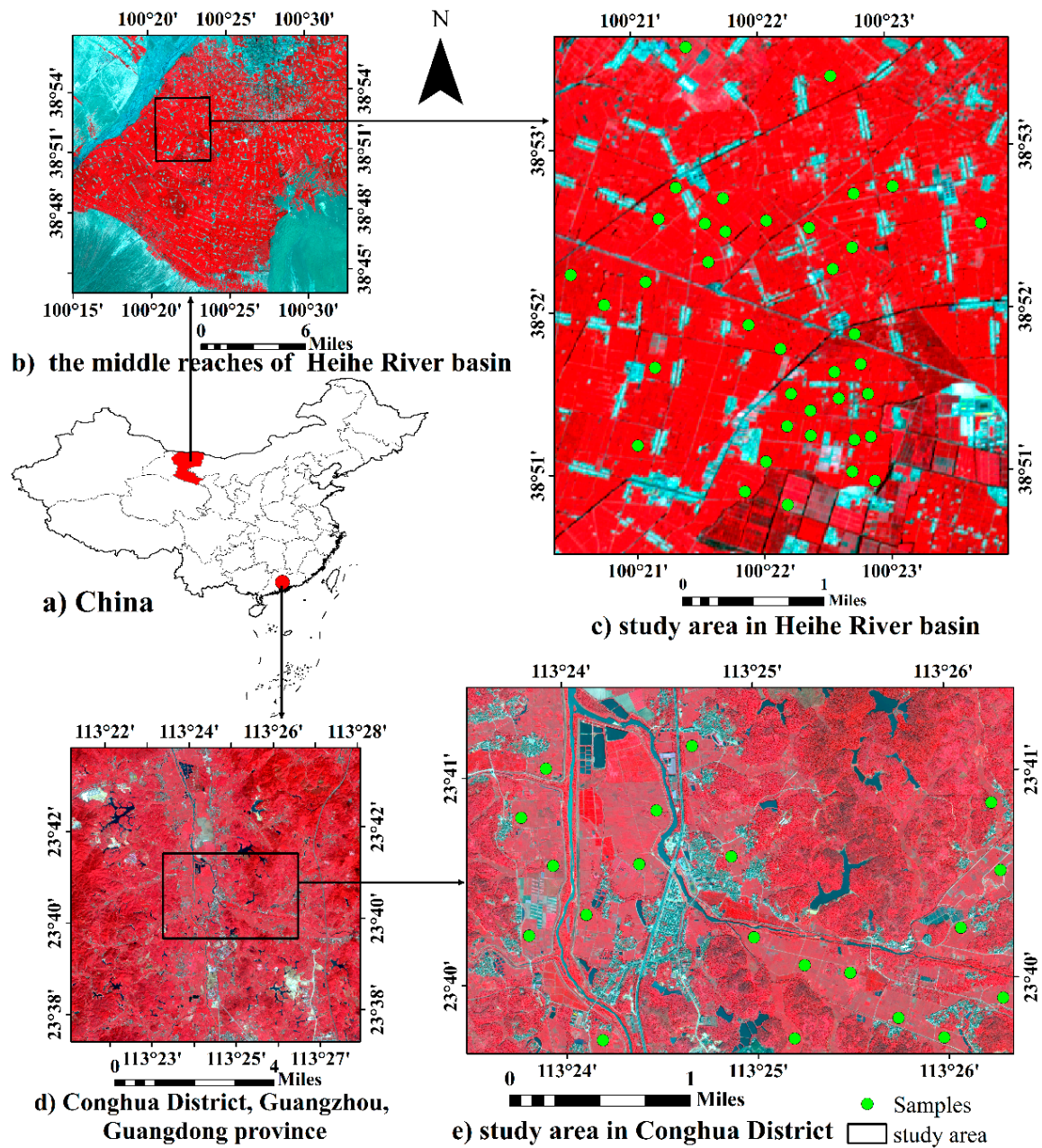
Figure 1. The location of the study areas shown using a false color composite image from ASTER data and GF-1 data: (**a**) China; (**b**) the middle reaches of Heihe River Basin; (**c**) study area in Heihe River Basin; (**d**) Conghua District, Guangzhou, Guangdong Province; (**e**) study area in Conghua District.

2.3. Methods

2.3.1. Leaf area index Reference Maps Generated Using the PROSAIL Model

To produce LAI reference maps (15 m ASTER and 8 m GF-1 LAI), it is critical to construct an estimation model. In this estimation model, the LAI is the dependent variable while canopy reflectance are the independent variables [24]. The empirical estimation model can be written as [25]:

$$\hat{y} = a + \sum_{i=1}^{n} b_i \cdot x(\lambda_i) \tag{1}$$

where the dependent variable ($\hat{y}$) is the estimated value of LAI of reference maps; a and b represent constant values; $x(\lambda_i)$ represents the optimal relevant canopy reflectance at wavelength λ_i; and n is the total number of canopy reflectance variables. Multiple linear regression (MLR) was used to construct the empirical estimation model.

The field measured LAI in the study area were not sufficient for building an empirical model for deriving the ASTER and GF-1 LAI reference maps. Thus, we simulated ground LAI with the PROSAIL model, coupled by the leaf optical properties model PROSPECT [24] and the vegetation canopy model SAIL [25]. The PROSPECT model is expressed as [26]:

$$(\rho_1, \tau_1) = \text{PROSPECT}(N, Cab, Cbrown, Car, Cw, Cm) \tag{2}$$

where N is a leaf structure parameter (unitless); Cab is the chlorophyll a and b content ($\mu g/cm^2$); $Cbrown$ is the brown pigment content ($\mu g/cm^2$); Car is the carotenoid content ($\mu g/cm^2$); Cw is the water content(g/cm^2); and Cm is the dry matter content($\mu g/cm^2$). The SAIL model is written as [27]:

$$\rho = \text{SAIL}(\rho_1, \tau_1, LAI, LAD, \rho soil, Diff, Hspot, SZA, VZA, RAA) \tag{3}$$

where the input parameters are leaf reflectance ρ_1; transmittance τ_1; leaf area index LAI; leaf inclination distribution LAD; diffuse reflection coefficient Diff; soil coefficient ρsoil; hot spot parameter Hspot; atmosphere conditions and view-illumination geometry (solar zenith angle (SZA); view zenith angle (VZA); and relative azimuth angle (RAA).

In this study, qualitative and quantitative sensitivity analysis methods were driven to obtain sensitive parameters, as shown in Figures 2 and 3. The qualitative sensitivity analysis was performed by observing the change of the simulated top-of-the-canopy reflectance curves when varying one parameter while keeping the other parameters constant [28]. The quantitative sensitivity method used the sensitivity formula to obtain sensitivity parameters. The sensitivity (S) formula is as follows [28,29]:

$$S = \frac{\sum_{j=1}^{n}\left(\rho_{Xo}^{(j)} - \rho_{Xo+\Delta X}^{(j)}\right)^2}{\rho_{Xo}^{(j)}} \tag{4}$$

where X_o is the original parameter value of the model; ΔX is the parameter step, which was determined through the PROSAIL model test according to relevant references [28]; $\rho_{Xo}^{(j)}$ is the original canopy reflectance of the jth added step; $\rho_{Xo+\Delta X}^{(j)}$ is the simulated canopy reflectance when the jth parameter value is $X + \Delta X$; and n is the number of added steps.

Figure 2 shows that the variation of the Cab curve was the largest in the range of 500 nm~700 nm, followed by LAD. In the range of 760 nm~1300 nm, the parameters LAI, LAD, SZA, VZA, Hspot, and Cm had a significant influence on canopy reflectance. In the range of 2080 nm~2350 nm, the curve variation of LAD, LAI SZA, and VZA were relatively larger. The parameters Car, Cbrown, ρsoil, Diff, and RAA had weak sensitivity in all wavebands.

Figure 3 shows that Cab was the most sensitive parameter in the range of 500 nm to 700 nm, the sensitivity of LAI was more significant than other parameters in the range of 720 nm to 1300 nm, and the LAD was also a sensitive parameter from 720 nm to 2500 nm. Therefore, Cab, LAI, and LAD were selected as sensitive parameters of the PROSAIL model. The specific ranges for the input parameters in the PROSAIL model set in this study are shown in Table 1.
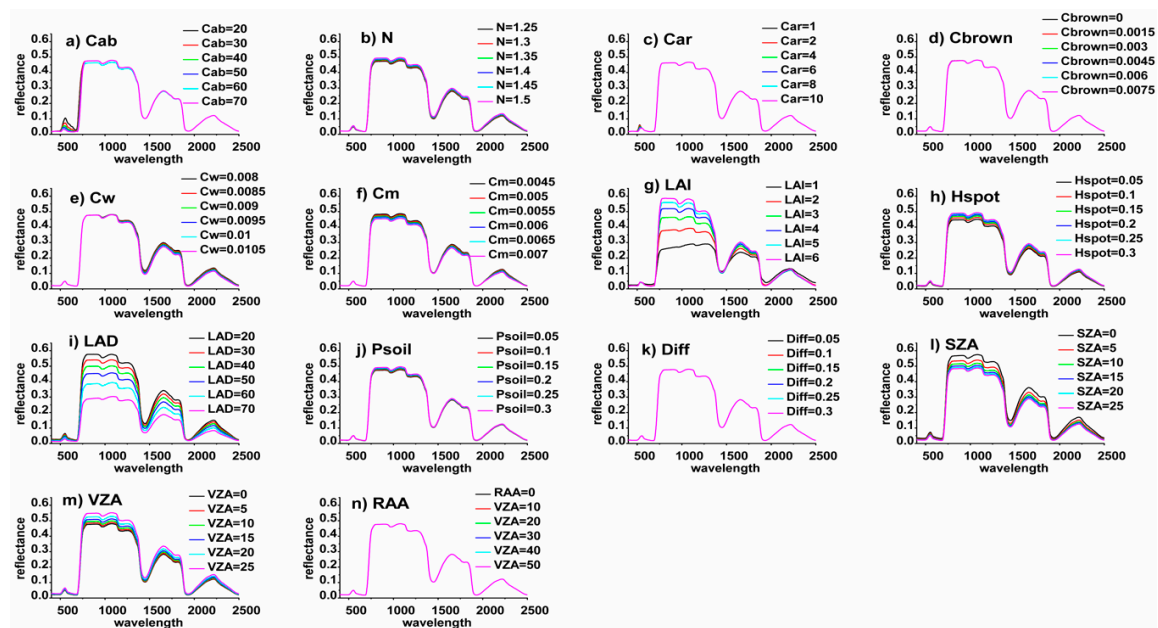
Figure 2. Influence of the input parameters on canopy reflectance in the PROSAIL model.
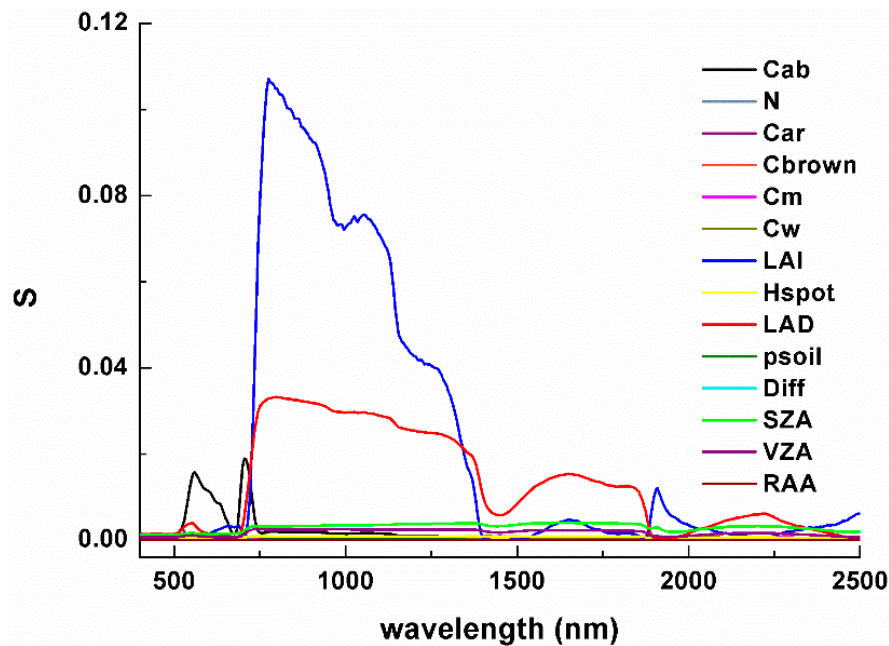

Figure 3. The sensitivities of the parameters in the PROSAIL model: the blue, red and black line indicate the sensitivities of LAI, LAD and Cab, respectively.

After deciding the input parameter values, the PROSAIL model was driven to generate the look-up-table (LUT) using the simulated LAI and corresponding canopy reflectance. In the LUT, one LAI value corresponded to 2101 canopy reflectance data from 2101 bands from 400 nm to 2500 nm. Therefore, in order to obtain an accurate empirical estimation model of LAI (Equation (1)), the appropriate canopy reflectance bands need to be determined from the 2101 bands, according to the Pearson correlation coefficient and significance level. In this study, the accurate empirical estimation model of LAI was constructed, taking LAI in the LUT as the dependent variable and the corresponding canopy reflectance of appropriate bands as independent variables.

Table 1. The input parameters setting in the PROSAIL model.

Parameters	Units	Min	Max	Step
leaf structure index N	unitless	1.3	1.3	-
leaf chlorophyll content a + b Cab	$(\mu g/cm^2)$	20	70	5
carotenoid content Car	$(\mu g/cm^2)$	8	8	-
brown pigment Cbrown	$(\mu g/cm^2)$	0	0	-
water content Cw	(g/cm^2)	0.0095	0.0095	-
dry matter content Cm	$(\mu g/cm^2)$	0.0015	0.0015	-
leaf area index LAI	(m^2/m^2)	0.05	7	0.05
hot parameter Hspot	(m^2/m^2)	0.2	0.2	-
leaf angle distribution LAD	(°)	20	70	5
diffuse reflection coefficient Diff	(fraction)	0.2	0.2	-
soil coefficient ρsoil	unitless	0.5	0.5	-
Sun zenith angle SZA	(°)	32	32	-
view zenith angle VZA	(°)	0	0	-
Relative azimuth angle RAA	(°)	0	0	-

2.3.2. Validation of Multi-Scale MODIS LAI Products Based on the EBK Interpolation

The LAI products must be compared under the same spatial scale. Therefore, as a robust non-stationary algorithm for spatial interpolating geophysical corrections [30], the EBK interpolation in this study performed downscaling transformation on 500 m MODIS LAI products and upscaling transformation on the LAI reference maps to conduct the validation of multi-scale MODIS LAI products. In the EBK method, the expression of the predicted LAI values by Kriging $Z_{(x_0)}$ is as follows [31,32]:

$$Z_{(x_0)} = \sum_{i=1}^{n} \lambda_i \cdot Z_{(x_i)} + \sum_{i=1}^{n} s_i \cdot U_{(x_i)} \tag{5}$$

where Z_1, Z_2, Z_3 ... Z_n are the field measured LAI values; $\lambda_i (i = 1,2,3 ... n)$ are kriging weights estimated using parameters of the cross-variograms; and $s_i (i = 1,2,3 ... n)$ are kriging weights estimated on the basis of a cross-variogram between $Z_{(x_i)}$ and $U_{(x_i)}$. n denotes the total number of observations, where n represents 182 and 135,192 for 500 m MODIS LAI product and 15 m ASTER LAI in Heihe River Basin study area, respectively, and 140 and 276,219 for 500 m MODIS LAI product and 8 m GF-1 LAI in the Conghua study area. The variable $U_{(x)}$ was a standardized rank that was calculated as [33]:

$$U_{(x_i)} = \frac{R}{n} \tag{6}$$

where R is a rank of the Rth order statistic of LAI measured on the land surface at location x_i.

In this study, EBK interpolation was performed as an upscaling transformation of the 15 m ASTER and 8 m GF-1 LAIs to 500 m reference maps. The 500 m MODIS LAI products were then respectively downscaled to 15 m and 8 m. At the validation stage, the measured LAI data and satellite (MODIS, GF-1, and ASTER) LAI with the same resolution were compared to each other to validate the reliability of the 500 m MODIS LAI products at different spatial scales. Four statistical metrics (the determination coefficient R^2, mean relative error MRE, root-mean-square error RMSE and relative root mean square error RRMSE) were used to quantify the deviation between two datasets:

$$R^2 = 1 - \frac{\sum_{i=1}^{n}\left(y_i - \hat{y}_i\right)^2}{\sum_{i=1}^{n}\left(y_i - \overline{y}_i\right)^2} \tag{7}$$

$$MRE = \frac{\sum_{i=1}^{n}\left|y_i - \hat{y}_i\right|/y_i}{n} \tag{8}$$

$$RMSE = \sqrt{\frac{\Sigma_{i=1}^{n}\left(y_i - \hat{y}_i\right)^2}{n}} \tag{9}$$

$$RRMSE = \frac{RMSE}{\overline{y}} \times 100\% \tag{10}$$

where $\overline{y}$ is the mean value of the measured samples; y_i is the measured value of the ith sample; $\hat{y}_i$ is the estimated value of the ith sample; and n is the number of samples.

3. Results

3.1. Distribution Map of Multi-Scale ASTER, GF-1, and MODIS LAI over Crop during Its Growth Cycle

The Pearson correlation coefficients between the field simulated LAI and field measured spectral canopy reflectance are shown in Figure 4, which indicates that band 824 nm had the largest correlation with LAI compared to other spectral bands. Therefore, in this paper, the ASTER band 3, with a range of 760 nm–860 nm, was selected to create the ASTER LAI products at 15 m resolution.
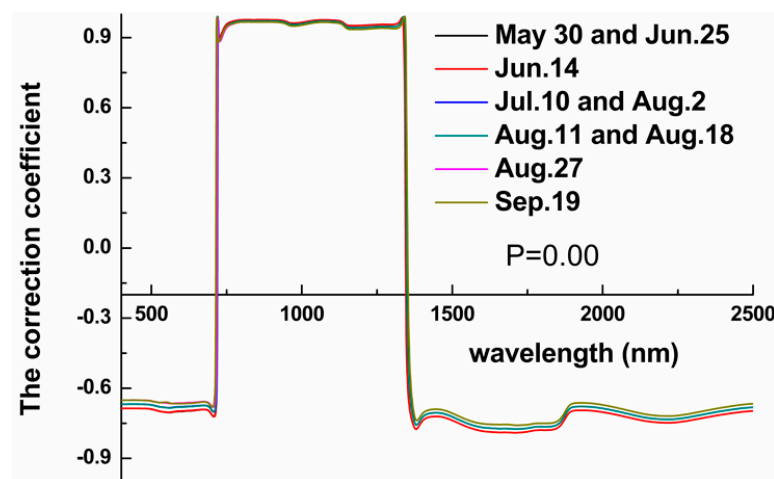

Figure 4. Pearson correlation coefficients between the field simulated leaf area index and field measured canopy reflectance.

The canopy reflectance data simulated by the PROSAIL model were spectrally resampled by the spectral resampling model in ENVI 5.3 to correspond to the spectral resolution (760–860 nm) of ASTER band 3. Then, the LUT was constructed by the resampled canopy reflectance data and LAI simulated by the PROSAIL model, which was used to solve the coefficients of Equation (1). Finally, the ASTER LAI and GF-1 LAI products with 15 m and 8 m spatial resolution were generated according to Equation (1), which is shown in the left figure of each phase in Figures 5 and 6. At the same time, the EBK interpolation method was driven to perform the downscaled transformation of the 500 m MODIS LAI products to generate MODIS LAI products at 15 m and 8 m resolution, which is shown in the right figure of each phase in Figures 5 and 6.

As shown in the left figure of each phase in Figures 5 and 6, LAI increased first and then decreased with time during the growth cycle of crops (corn and rice). LAI values were small at the early growing period (30 May and 14 June for corn; 3 August for rice), shown in red and orange shades in the graphs. LAI values began to increase at the middle stage (mid-to-late July and early August for corn and late September for rice) and peaked at the heading to flowering stage (mid-August for corn; 15 October for rice). Later, LAI values began to decrease at the maturity stage (mid-to-late September for corn and mid-to-late October for rice). During the crop growth cycle, the ASTER-derived LAI distribution maps were basically consistent with those of MODIS. While there was relatively larger difference in the early

and late growth stage because 15 m MODIS products were acquired from 500 m MODIS products having more many mixed pixels than the other phases in the corn and rice fields.
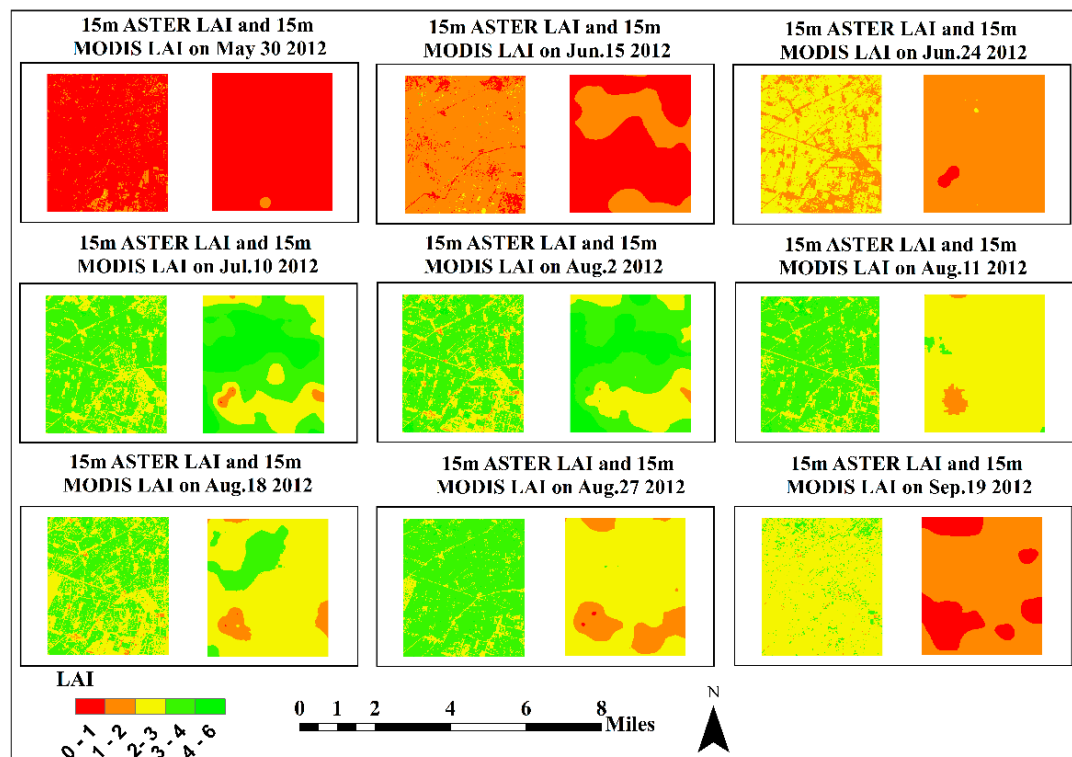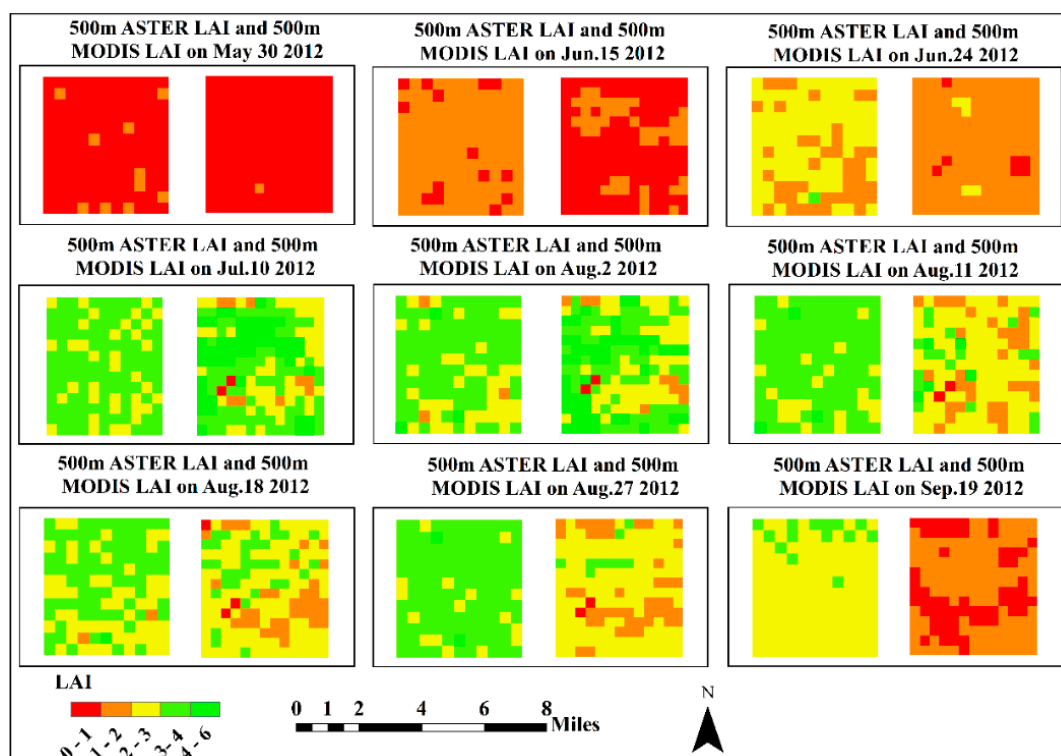

Figure 5. The time series distribution map of 15 m ASTER LAI (left figure of each period) and MODIS LAI with 15 m resolution interpolated by the EBK method (right figure of each period) during the growth cycle of corn.
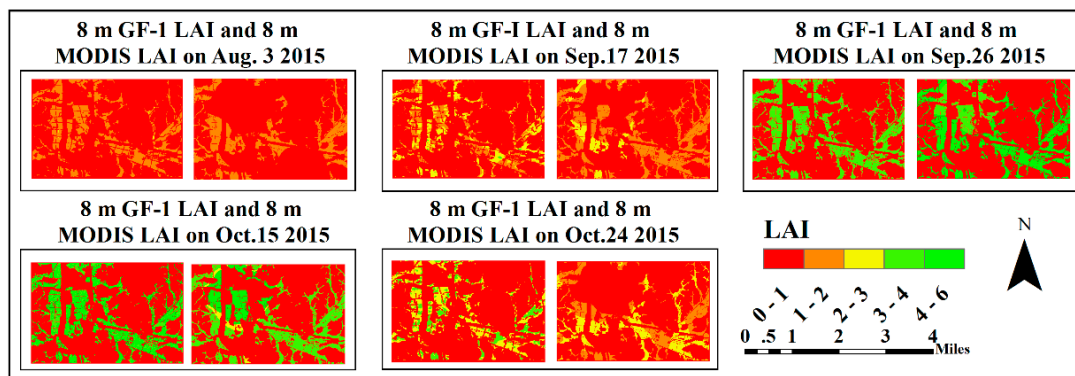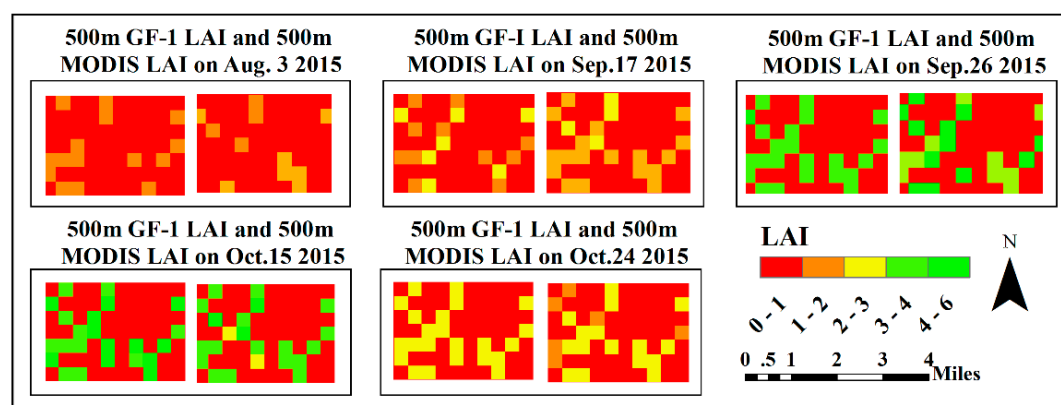

Figure 6. The time series distribution map of 8 m GF-1 (left figure of each period) and MODIS LAI with 8 m resolution interpolated by the EBK method (right figure of each period) during the growth cycle of rice.

The EBK interpolation method was used to perform the upscaling transformation of 15 m ASTER and 8 m GF-1 LAI to LAI products at 500 m resolution, respectively, which are shown in the left figure of each period in Figures 7 and 8. The 500 m LAI products obtained by the EBK method lost detailed information (such as roads and villages) as pixels became mixed. From the spatial distributions of LAI in Figures 5–8, the 500 m ASTER and GF-1 LAI were more consistent with the 500 m MODIS LAI products than other 15 m and 8 m LAI products with more detailed information. The frequency distribution (Figure 9) also indicates that more detailed spatial LAI patterns could be found in downscaled LAI, but were averaged out in the original MODIS LAI.

Figure 7. Time series distribution map of 500 m ASTER LAI (left figure of each period) interpolated by the EBK method and MODIS LAI with 500 m resolution (right figure of each period) during the corn growth cycle.


Figure 8. Time series distribution map of 500 m GF-1 LAI (left figure of each period) interpolated by the EBK method and MODIS LAI with 500 m resolution (right figure of each period) during the rice growth cycle.

3.2. Multi-Scale Validation of MODIS LAI Product

For this study, 121 and 100 in situ LAI measurements were collected in Heihe River Basin and Conghua District, respectively, during the crop growth cycle to validate the LAI products. The MODIS LAI products at 8 m, 15 m, and 500 m spatial resolution were compared with ASTER LAI products at 15 m and 500 m resolution, with GF-1 LAI products at 8 m and 500 m resolution and with the field measured LAI (shown in Figure 10). Figure 10 highlights the differences among MODIS LAI, ASTER LAI, GF-1 LAI, and measured LAI. In Figure 10, compared to the field measured LAI and ASTER LAI during the crop growth cycle, MODIS LAI tends to underestimate at low LAI and overestimate at high LAI. ASTER LAI values at 15 m resolution were closer to the MODIS LAI values than the field measured LAI values because of decreased spatial scale mismatch between the two pixel-based products.
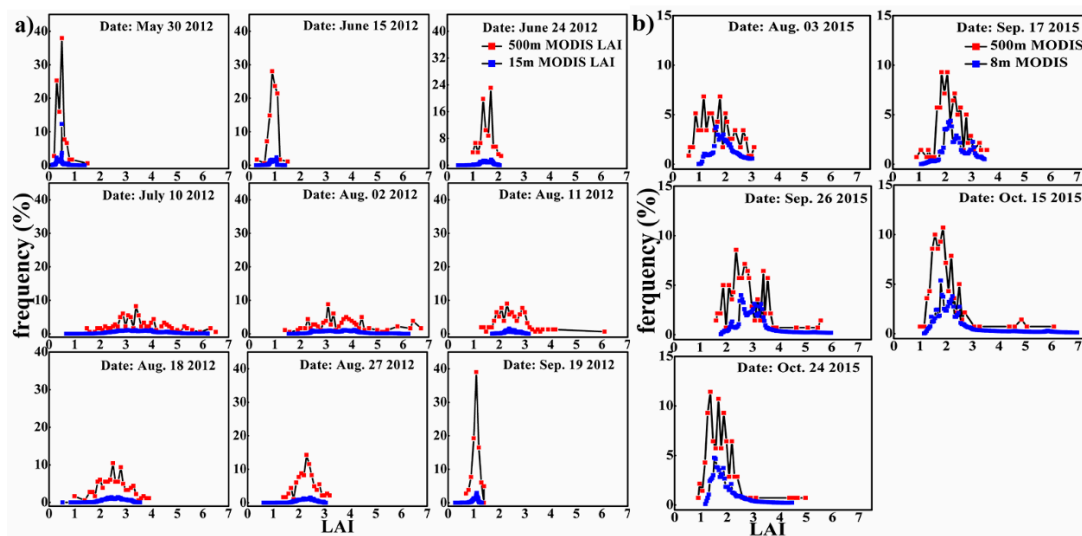
Figure 9. The time series frequency distribution: (**a**) 15 m MODIS LAI and MODIS LAI with 500 m resolution during the growth cycle of corn, (**b**) 8 m MODIS LAI and MODIS LAI with 500 m resolution during the growth cycle of rice.
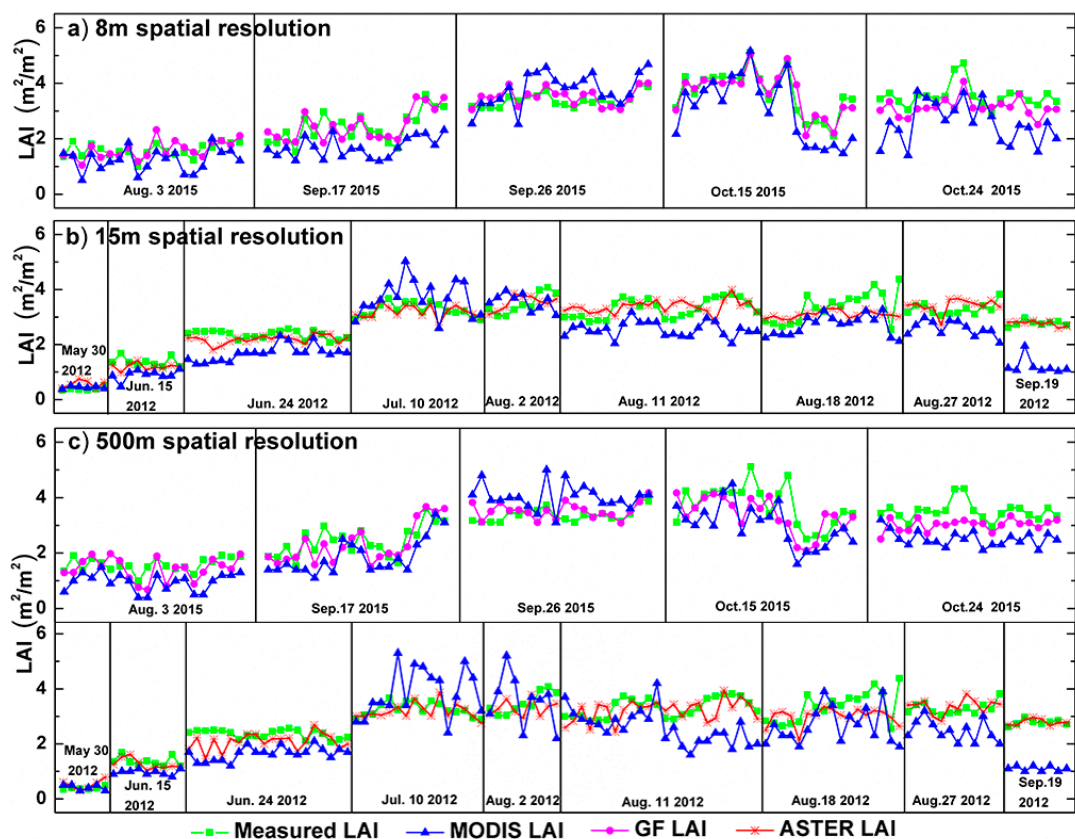
Figure 10. Sample comparison among MODIS LAI, ASTER LAI, GF-1 LAI, and field measured data during the crop growth cycle: (**a**) LAI products with 8 m resolution; (**b**) LAI products with 15 m resolution; (**c**) LAI products with 500 m resolution.

The MODIS LAI products, ASTER LAI products, GF-1 LAI products, and field measured LAI values from validation samples were compared by calculating the MRE, RMSE, and relative RMSE percentage (Figure 11). The highest R^2 was between MODIS LAI and ASTER LAI at 15 m resolution (R^2 = 0.758), followed by the correlation between MODIS LAI and measured LAI (R^2 = 0.745). The validation

accuracy of MODIS LAI using ASTER LAI was higher than GF-1 LAI and field measured LAI, showing that the RRMSE was 28.73% for 15 m resolution, 29.00% for 8 m resolution, and 29.41%–30.80% for 500 m resolution, respectively, which suggests that the ASTER LAI products generated by the PROSAIL model were more suitable to validate the MODIS LAI products. The MODIS LAI products at 15 m resolution were closer to the field measured LAI than the 500 m and 8 m resolution MODIS LAI products, which implies that the MODIS LAI products at 15 m resolution would be more effective in monitoring surface vegetation cover and vegetation growth.
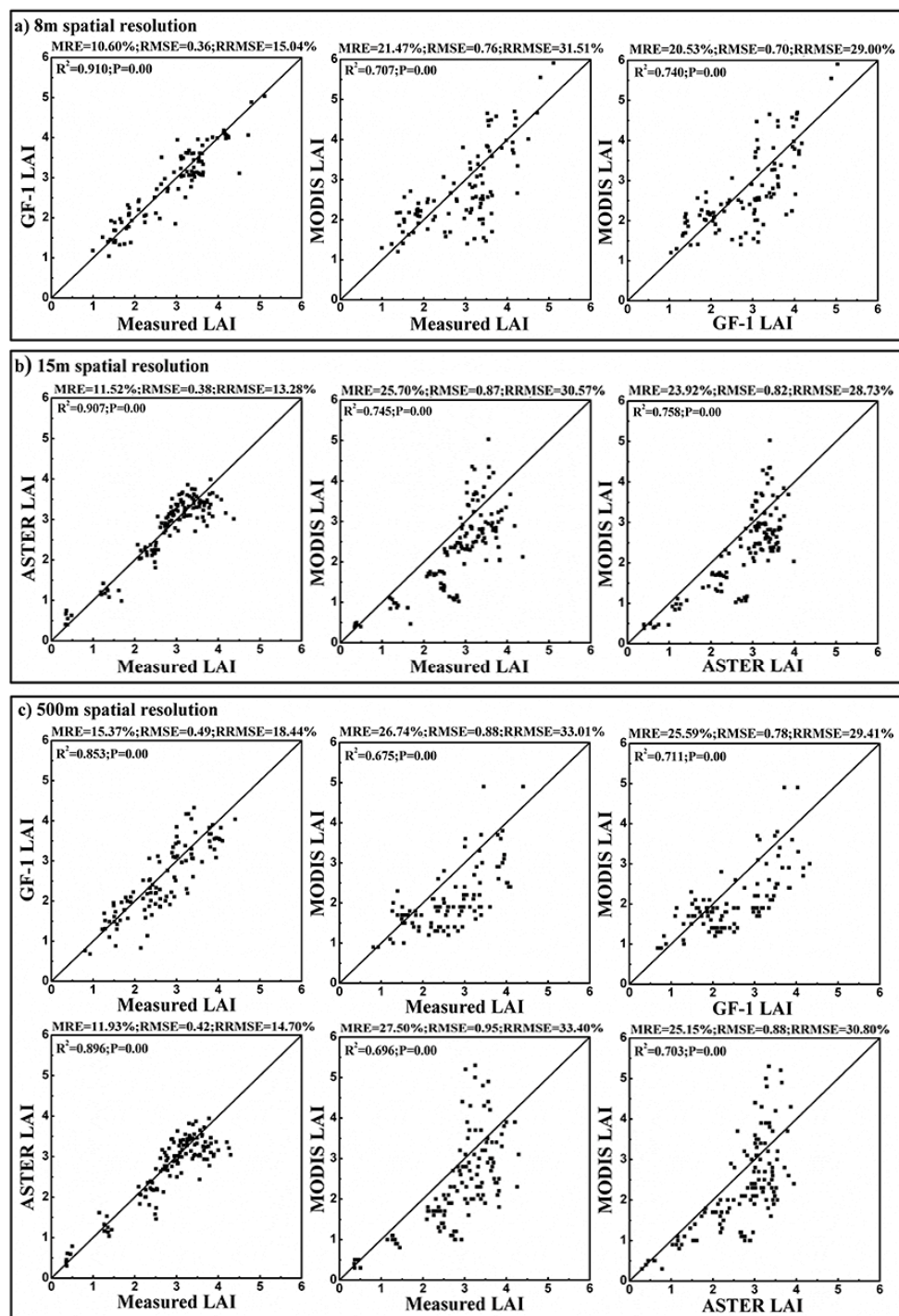
Figure 11. The LAI product versus LAI product scatter plots in the study areas using the corn and rice LAI values from the growth stages: (**a**) 8 m LAI product; (**b**) 15 m LAI product; (**c**) 500 m LAI product.

4. Discussion

4.1. Comparison with Other Similar Studies

Previous studies using direct and indirect methods to validate the accuracy of MODIS LAI products at a local or global scale [15,17,34–40], while providing valuable information, have some limitations.

First, previous validation methods [5,7] focused on validating MODIS LAI products at 500 m without downscaling the MODIS LAI to a finer resolution. Thus, these methods cannot evaluate the reliability of the 500 m MODIS LAI products at a fine local scale. The method proposed in this paper not only validated the accuracy of the MODIS LAI product with 500 m spatial resolution, but also validated the MODIS LAI with 15 m and 8 m spatial resolution generated by the EBK interpolation of the 500 m MODIS LAI. From Figure 11, the evaluation statistics derived from the comparison between the 15 m MODIS LAI and 15 m ASTER LAI were 0.758 of R^2, 23.92% of MRE, 0.82 of RMSE and 28.73% of RRMSE, which show improvements of 0.055, 1.23%, 0.06, and 2.07%, respectively, compared with the results calculated at 500 m spatial resolution. When compared to 8 m GF-1 LAI, the evaluation statistics of 8 m MODIS LAI products were 0.740 of R^2, 20.53% of MRE, 0.70 of RMSE, and 29.00% of RRMSE. These results show that the MODIS LAI with 15 m resolution obtained by EBK interpolation was more reliable than the MODIS LAI products with a 500 m resolution.

Second, previous validation studies [8,11] were based on a variety of vegetation types and rarely considered the crop growth cycle to validate the MODIS LAI product. In this study, the MODIS LAI products were validated based on the corn and rice growth cycles. Figure 10 indicates that the MODIS LAI product showed the mischaracterized corn and rice growth cycles except for the crop heading to the flower stage (August for corn and mid-October for rice), underestimating in low LAI regions and overestimating at LAI high regions. The results were in agreement with those of previous studies [17], where the inversion accuracy of the Collection 5 MODIS LAI (MOD15A2) products was examined for three typical vegetation types (i.e., alpine meadow, steppe, and subalpine shrub).

Third, though few downscaling techniques studies [19] have been able to downscale the lower spatial resolution satellite LAI products into the spatial resolution of the bridging LAI results and then conduct a comparison, some downscaling techniques have been applied to acquire other remote sensing data estimates [41,42]. Three machine learning approaches—random forest, boosted regression trees, and Cubist—were evaluated for a downscaling of the 25 km AMSR-E soil moisture data using 1 km MODIS products with a R^2 ranging from 70% to 75% [41]. Compared with the EBK downscaling method, the predictive accuracy of these downscaling methods showed no obvious difference. Thus, to improve the product validation accuracy, the optimal algorithm will be sieved in the future.

4.2. Prospects for Future Studies

The proposed method serves as a reference for future validation work. Due to the absence of other field vegetation type information, we cannot currently validate the MODIS LAI product uncertainties brought about by the type of vegetation. Thus, more field measured samples from different vegetation types need to be collected to further validate the reliability of the proposed validation method.

In this study, the scale-transformation method was performed between 500 m, 15 m, and 8 m spatial resolution pixels, which affects the accuracy of the validation due to the large difference in spatial scales. Future studies should consider introducing intermediate spatial scales of LAI to complete the MODIS LAI validation.

5. Conclusions

This study validated the MOD15A2H LAI products using a new multi-scale LAI product validation method based on the crop growth cycle. The experiment was conducted by long-term in situ observations during the corn and rice growth cycles. Results have shown that the MODIS LAI product with 500 m spatial resolution was overestimated during the medium growth stage (mid-to-late July and early August for corn and late September for rice) and underestimated during other growth stages

(including tillering stage, jointing stage, heading to flowering stage, and maturity stage). The ASTER LAI values obtained by the PROSAIL model were more closely related to the MODIS LAI than GF-1 LAI and field measured LAI, with a R^2 of 0.758 for 15 m spatial resolution, and R^2 of 0.703 for 500 m. The relationship between MODIS LAI and field measured LAI had R^2 of 0.707 for 8 m, R^2 of 0.745 for 15 m, and R^2 of 0.675–0.696 for 500 m. Uncertainties in current satellite products still exist at different scales. Future studies should focus on considering the scale difference between field measurements and moderate resolution pixels utilizing higher resolution and pure pixel information of vegetation type observations.

Author Contributions: Z.L. and T.W. conceived and designed the experiments; T.W. analyzed the data, created the tables and figures, and finished the first version of the paper; Z.L., T.W., Y.Q., Ziqing Xia, and Y.P. contributed valuable opinions during the manuscript writing; Z.L. and Y.Q. revised the whole manuscript. All authors read and approved the final manuscript.

Conflicts of Interest: The authors declare no conflicts of interest.

References

1. Moran, M.S.; Maas, S.J.; Pinter, P.J. Combining remote sensing and modeling for estimating surface evaporation and biomass production. *Remote Sens. Rev.* **1995**, *12*, 335–353. [CrossRef]
2. Norman, J.M.; Kustas, W.P.; Humes, K.S. Source approach for estimating soil and vegetation energy fluxes in observations of directional radiometric surface temperature. *Agric. For. Meteorol.* **1995**, *77*, 263–293. [CrossRef]
3. Anderson, M.C.; Norman, J.M.; Kustas, W.P.; Li, F.; Prueger, J.H.; Mecikalski, J.R. Effects of Vegetation Clumping on Two–Source Model Estimates of Surface Energy Fluxes from an Agricultural Landscape during SMACEX. *J. Hydrometeorol.* **2005**, *6*, 892–909. [CrossRef]
4. Doraiswamy, P. Crop condition and yield simulations using Landsat and MODIS imagery. *Remote Sens. Environ.* **2004**, *92*, 548–559. [CrossRef]
5. Sun, C.; Liu, L.; Guan, L.; Jiao, Q.; Peng, D. Validation and error analysis of the MODIS LAI product in Xilinhot grassland. *J. Remote Sens.* **2014**, *18*, 518–536.
6. Morisette, J.T.; Baret, F.; Privette, J.L.; Myneni, R.B.; Nickeson, J.E.; Garrigues, S.; Shabanov, N.V.; Fernandes, R.A.; Leblanc, S.G.; Kalacska, M.; et al. Validation of global moderate-resolution LAI products: A framework proposed within the CEOS land product validation subgroup. *IEEE Trans. Geosci. Remote Sens.* **2006**, *44*, 1804–1817. [CrossRef]
7. Garrigues, S.; Lacaze, R.; Baret, F.; Morisette, J.T.; Weiss, M.; Nickeson, J.E.; Fernandes, R.; Plummer, S.; Shabanov, N.V.; Myneni, R.B.; et al. Validation and intercomparison of global Leaf Area Index products derived from remote sensing data. *J. Geophys. Res. Biogeosciences* **2008**, *113*. [CrossRef]
8. Fang, H.; Wei, S.; Liang, S. Validation of MODIS and CYCLOPES LAI products using global field measurement data. *Remote Sens. Environ.* **2012**, *119*, 43–54. [CrossRef]
9. Yang, Y.; Li, A.; Jin, H.; Yin, G.; Zhao, W.; Lei, G.; Bian, J. Intercomparison Among GEOV1, GLASS and MODIS LAI Products over Mountainous Area in Southwestern China. *Remote Sens. Technol. Appl.* **2016**, *31*, 438–450.
10. Gessner, U.; Niklaus, M.; Kuenzer, C.; Dech, S. Intercomparison of leaf area index products for a gradient of sub-humid to arid environments in West Africa. *Remote Sens.* **2013**, *5*, 1235–1257. [CrossRef]
11. Jin, H.; Li, A.; Bian, J.; Nan, X.; Zhao, W.; Zhang, Z.; Yin, G. Intercomparison and validation of MODIS and GLASS leaf area index (LAI) products over mountain areas: A case study in southwestern China. *Int. J. Appl. Earth Obs. Geoinf.* **2017**, *55*, 52–67. [CrossRef]
12. Sea, W.B.; Choler, P.; Beringer, J.; Weinmann, R.A.; Hutley, L.B.; Leuning, R. Documenting improvement in leaf area index estimates from MODIS using hemispherical photos for Australian savannas. *Agric. For. Meteorol.* **2011**, *151*, 1453–1461. [CrossRef]
13. Zeng, Y.; Li, J.; Liu, Q. Review article: Global LAI ground validation dataset and product validation framework. *Adv. Earth Sci.* **2012**, *27*, 165–174.

14. Liu, Y.; Wang, J.; Zhou, H.; Xue, H. Upscaling approach for validation of LAI products derived from remote sensing observation. *J. Remote Sens.* **2014**, *18*, 1189–1198.

15. Yin, G.; Li, A.; Jin, H.; Zhao, W.; Bian, J.; Qu, Y.; Zeng, Y.; Xu, B. Derivation of temporally continuous LAI reference maps through combining the LAI Net observation system with CACAO. *Agric. For. Meteorol.* **2017**, *233*, 209–221. [CrossRef]

16. Liu, L. Simulation and correction of spatialscaling effects for leaf area index. *J. Remote Sens.* **2014**, *18*, 1158–1168.

17. Yang, J.; Chen, H.; Borjigin, N.; Zhao, M.; Zhou, Y.; Huang, Y. Validation of the MODIS LAI product in Qinghai Lake Basin combined with field measurements using Landsat 8 OLI data. *Acta Ecol. Sin.* **2017**, *37*, 322–331. [CrossRef]

18. Liu, Z.; Huang, R.; Hu, Y.; Fan, S.; Feng, P. Generating high spatiotemporal resolution LAI based on MODIS/GF-1 data and combined kriging-cressman interpolation. *Int. J. Agric. Biol. Eng.* **2016**, *9*, 120–131.

19. Houborg, R.; Mccabe, M.F.; Gao, F. A Spatio-Temporal Enhancement Method for medium resolution LAI (STEM-LAI). *Int. J. Appl. Earth Obs. Geoinf.* **2016**, *47*, 15–29. [CrossRef]

20. Qu, Y.; Zhu, Y.; Han, W.; Wang, J.; Ma, M. Crop leaf area index observations with a wireless sensor network and its potential for validating remote sensing products. *IEEE J. Sel. Top. Appl. Earth Obs. Remote Sens.* **2014**, *7*, 431–444. [CrossRef]

21. Li, X.; Liu, S.; Xiao, Q.; Ma, M.; Jin, R.; Che, T.; Wang, W.; Hu, X.; Xu, Z.; Wen, J.; et al. A multiscale dataset for understanding complex eco-hydrological processes in a heterogeneous oasis system. *Sci. Data* **2017**, *4*, 170083. [CrossRef] [PubMed]

22. Available online: http://www.heihedata.org (accessed on 10 October 2019).

23. LP DAAC - MOD15A2H. Available online: https://lpdaac.usgs.gov/products/mod15a2hv006/ (accessed on 20 October 2019).

24. Kancheva, R.; Georgiev, G. Assessing Cd-induced stress from plant spectral response. In Proceedings of the SPIE—The International Society for Optical Engineering, Amsterdam, The Netherlands, 22–25 September 2014; Volume 9239, pp. 1–12.

25. Krzywinski, M.; Altman, N. Multiple linear regression. *Nat. Methods* **2015**, *66*, 1103–1104. [CrossRef] [PubMed]

26. Feret, J.B.; François, C.; Asner, G.P.; Gitelsond, A.A.; Martin, R.E.; Bidel, L.P.R.; Ustin, S.L.; Maire, G.; Jacquemoud, S. PROSPECT-4 and 5: Advances in the leaf optical properties model separating photosynthetic pigments. *Remote Sens. Environ.* **2008**, *112*, 3030–3043. [CrossRef]

27. Jacquemoud, S.; Verhoef, W.; Baret, F.; Bacour, C.; Zarco-Tejada, P.J.; Asner, G.P.; François, C.; Ustin, S.L. PROSPECT + SAIL models: A review of use for vegetation characterization. *Remote Sens. Environ.* **2009**, *113*, S56–S66. [CrossRef]

28. Gu, C.; Du, H.; Zhou, G.; Han, N.; Xu, X.; Zhao, X.; Sun, X. Retrieval of leaf area index of Moso bamboo forest with Landsat Thematic Mapper image based on PROSAIL canopy radiative transfer model. *Chin. J. Appl. Ecol.* **2013**, *24*, 2248–2256.

29. Li, H. Leaf Area Index Retrieval Based on Prospect, Liberty and Geosail Models. *Sci. Silvae Sin.* **2011**, *47*, 75–81.

30. Krivoruchko, K.; Butler, K. *Unequal Probability-Based Spatial Sampling*; Esri: Redlands, CA, USA, 2013.

31. Goovaerts, P. Kriging and Semivariogram Deconvolution in the Presence of Irregular Geographical Units. *Math. Geosci.* **2008**, *40*, 101–128. [CrossRef]

32. Omre, H. Bayesian kriging-merging observations and qualified guesses in kriging. *Math. Geol.* **1987**, *19*, 25–39. [CrossRef]

33. Fabijańczyk, P.; Zawadzki, J.; Magiera, T. Magnetometric assessment of soil contamination in problematic area using empirical Bayesian and indicator kriging: A case study in Upper Silesia, Poland. *Geoderma* **2017**, *308*, 69–77. [CrossRef]

34. John, I.; Russell, C.; Timothy, L.; Andrew, P. Uncertainty Analysis in the Creation of a Fine-Resolution Leaf Area Index (LAI) Reference Map for Validation of Moderate Resolution LAI Products. *Remote Sens.* **2015**, *7*, 1397–1421.

35. Claverie, M.; Weiss, M.; Frédéric, B.; Hagolle, O.; Demarez, V. Validation of coarse spatial resolution LAI and FAPAR time series over cropland in southwest France. *Remote Sens. Environ.* **2013**, *139*, 216–230. [CrossRef]

36. Serbin, S.P.; Ahl, D.E.; Gower, S.T. Spatial and temporal validation of the MODIS LAI and FPAR products across a boreal forest wildfire chronosequence. *Remote Sens. Environ.* **2013**, *133*, 71–84. [CrossRef]

37. Jia, S.; Ma, M.; Yu, W. Validation of the LAI Product in Heihe River Basin. *Remote Sens. Technol. Appl.* **2014**, *29*, 1037–1045.

38. Qu, Y.; Han, W.; Ma, M. Retrieval of a Temporal High-Resolution Leaf Area Index (LAI) by Combining MODIS LAI and ASTER Reflectance Data. *Remote Sens.* **2015**, *7*, 195–210. [CrossRef]

39. Myneni, R.B.; Hoffman, S.; Knyazikhin, Y.; Privette, J.L.; Glassy, J.; Tian, Y.; Wang, Y.; Song, X.; Zhang, Y.; Smith, G.R.; et al. Global products of vegetation leaf area and fraction absorbed PAR from year one of MODIS data. *Remote Sens. Environ.* **2002**, *83*, 214–231. [CrossRef]

40. Liu, Y.; Liu, R.; Chen, J.; Cheng, X.; Zheng, G. Current Status and Perspectives of Leaf Area Index Retrieval from Optical Remote Sensing Data. *Geo-Inf. Sci.* **2013**, *15*, 734. [CrossRef]

41. Jing, W.; Yang, Y.; Yue, X.; Zhao, X. A Spatial Downscaling Algorithm for Satellite-Based Precipitation over the Tibetan Plateau Based on NDVI, DEM, and Land Surface Temperature. *Remote Sens.* **2016**, *8*, 655. [CrossRef]

42. Im, J.; Park, S.; Rhee, J.; Baik, J.; Choi, M. Downscaling of AMSR-E soil moisture with MODIS products using machine learning approaches. *Environ. Earth Sci.* **2016**, *75*, 1120. [CrossRef]